In situ analysis of the structural transformation of glassy carbon under compression at room temperature

T. B. Shiell,[1,*] C. de Tomas,[2] D. G. McCulloch,[3] D. R. McKenzie,[4] A. Basu,[5] I. Suarez-Martinez,[2] N. A. Marks,[2] R. Boehler,[5,6] B. Haberl,[6] and J. E. Bradby[1]

[1]*Research School of Physics and Engineering, The Australian National University, Canberra, ACT 2601, Australia*
[2]*Department of Physics and Astronomy, Curtin University, Perth, WA 6845, Australia*
[3]*Physics, School of Science, RMIT University, Melbourne, VIC 3001, Australia*
[4]*School of Physics, The University of Sydney, Sydney, NSW 2006, Australia*
[5]*Geophysical Laboratory, Carnegie Institute of Washington, 5251 Branch Road NW, Washington, DC 20015, USA*
[6]*Neutron Scattering Division, Neutron Sciences Directorate, Oak Ridge National Laboratory, Oak Ridge, TN 37831, USA*

(Received 18 October 2018; revised manuscript received 23 December 2018; published 30 January 2019)

Room temperature compression of graphitic materials leads to interesting superhard sp^3 rich phases which are sometimes transparent. In the case of graphite itself, the sp^3 rich phase is proposed to be monoclinic M-carbon; however, for disordered materials such as glassy carbon the nature of the transformation is unknown. We compress glassy carbon at room temperature in a diamond anvil cell, examine the structure *in situ* using x-ray diffraction, and interpret the findings with molecular dynamics modeling. Experiment and modeling both predict a two-stage transformation. First, the isotropic glassy carbon undergoes a reversible transformation to an oriented compressed graphitic structure. This is followed by a phase transformation at ∼35 GPa to an unstable, disordered sp^3 rich structure that reverts on decompression to an oriented graphitic structure. Analysis of the simulated sp^3 rich material formed at high pressure reveals a noncrystalline structure with two different sp^3 bond lengths.

DOI: 10.1103/PhysRevB.99.024114

I. INTRODUCTION

When graphite is compressed at room temperature (cold compression), it transforms to a transparent phase at pressures above ∼15 GPa [1–3]. The origin of the transparency has been attributed to the formation of sp^3 rich phases which have been proposed to be superhard [4–10]. Recent work has proposed a monoclinic phase (M-carbon) is the most likely candidate for this transparent phase to be formed from a graphite precursor [1,4,11]. The formation of M-carbon was proposed due to the fact that it was shown to be the easiest to form kinetically [12]. There are reports of transparency being induced by room temperature compression of disordered carbon precursors, such as glassy carbon (GC) [13–15], but its causes are not well understood and a structural model has not been proposed. One study conducted by Lin *et al.* compressed GC in a diamond anvil cell (DAC) without a pressure medium and observed the material *in situ* using carbon K-edge x-ray Raman spectroscopy. This showed that the $1s$ to π^* peak in the spectra (an indicator of sp^2 bonding) vanishes at a pressure of 44 GPa [16], suggesting the (reversible) formation of a pure sp^3 bonded carbon phase at this pressure. In another study by Yao *et al.* GC was compressed in a DAC with KBr and N_2 pressure media and was monitored *in situ* using Raman spectroscopy [10]. This work found that GC becomes transparent at a pressure of ∼30 GPa in the presence of a large uniaxial component and associated transparency with the change in bonding from sp^2 to sp^3 hybridization. Further work by Solopova *et al.* compressed GC in a DAC with a Ne pressure medium to 60 GPa and observed the material *in situ* using Raman spectroscopy [17]. In contrast to the previous two studies, Solopova *et al.* found that the G peak in the Raman spectra (which is an indicator for sp^2 bonding) remains present up to 60 GPa. This challenges the assertion made by Lin *et al.* of a 100% conversion from sp^2 to sp^3 bonding at 44 GPa [16]. The reason for these discrepancies is unclear and it remains unknown how and at what pressure the sp^2 bonding in GC transforms to sp^3 bonding, *the* critical step for the formation of superhard carbon materials.

We have recently shown [18] using electron microscopy, Raman spectroscopy, and atomistic modeling that after loading GC in a DAC up to 35 GPa, the recovered material (i.e., measured *ex situ*) is found to retain its tangled nanostructure, including its minority content of sp^3 bonding (∼5%). However, samples recovered after compression to over 45 GPa contain a negligible sp^3 bonding content and permanent densification accompanied by a loss of the original nongraphitizing structure. This 45 GPa threshold represents the upper limit on the nongraphitizing and superelastic properties of GC, and was proposed to be the result of the formation of an unknown sp^3 rich phase which is unstable at ambient. In this previous study the nature of this high-pressure sp^3 bonded phase and the transformation pathway were not explored. Here we report the results of an *in situ* study, aided by molecular dynamics modeling, that aims to understand the nature of the transformation to the sp^3 rich phase formed with the ultimate aim of recovering a superhard material.

*tom.shiell@anu.edu.au

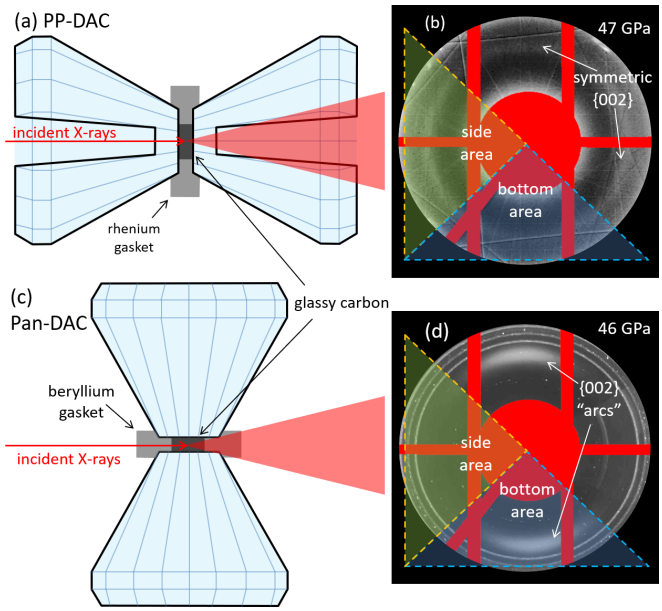

FIG. 1. (a) A schematic of the PP-DAC showing the incident x-ray beam aligned parallel to the compression direction. (b) An XRD pattern showing a symmetric {002} reflection onto the detector. The red areas indicate masking that has been applied to remove interference from the detector and beam stop. The triangular areas drawn on the diffraction patterns indicate the specific regions of the image that are integrated to form the spectra shown in Fig. 2. (c) A schematic of the pan-DAC with a beryllium gasket showing that the x-ray beam is incident perpendicular to the compression direction. (d) An XRD pattern showing a nonuniform {002} reflection onto the detector where the intensity is concentrated in two "arcs" aligned with the DAC compression axis. The sharp rings at the edges of the diffraction pattern are due to the beryllium gasket.

II. EXPERIMENT

The GC used in this study has a macroscopic density of 1.42 g/cm^3 (Sigradur-G, Hochtemperatur Werkstoffe). It was manufactured from a phenolic resin that was heated to 2500 °C. Small chips of appropriate size (∼150 × 150 × 70 μm) were selected for the present DAC experiments.

Two different types of DACs were used in these experiments. The first was a Boehler plate DAC [19] with specially fabricated partially perforated diamond anvils, which we refer to as the PP-DAC. This DAC was used to reduce the Compton scattering background from the diamond anvils during *in situ* x-ray diffraction (XRD) as shown in Fig. 1(a). Note *in situ* XRD was conducted with the incident x-ray beam parallel to the compression direction. The partial perforations, [achieved with a 193-nm excimer laser (GAM EX5)] reduce the diamond material penetrated by the x-ray beam from 2× ∼ 2 mm to 2× ∼ 200 μm. The anvils had culet diameters of 350 μm and were used with a rhenium gasket (170-μm-diameter hole, 65 μm thick). The GC sample was loaded without a pressure medium. The pressure in the cell was determined *in situ* by the shift of the rhenium peaks measured at the inner edge of the gasket.

The second type of DAC was a panoramic DAC (pan-DAC) as shown in Fig. 1(c). This was selected to conduct *in situ* XRD measurements with the incident x-ray beam perpendicular to the compression direction. The anvils in the pan-DAC had culet diameters of 300 μm and were used with a beryllium gasket (130-μm-diameter hole, 60 μm thick). Beryllium was used to minimize scattering from the gasket. As in the case of the PP-DAC, the GC sample was loaded into the pan-DAC without a pressure medium but with a ruby to be used for *in situ* pressure determination using the R1-ruby fluorescence line [20].

Note that there is an error associated with the measured pressure in these experiments due to the fact that a significant pressure gradient exists across the sample in the absence of a pressure transmitting medium. This means that the outer radial areas of the sample experience a lower pressure than the absolute center. Firstly, in the pan-DAC this results in the fact that the x-ray beam simultaneously scans through all regions even though they experience different pressures. This factor may have the effect of broadening the diffraction peaks slightly. Furthermore, in the pan-DAC the ruby pressure calibrant was placed in the center of the sample/gasket hole and thus corresponds to the maximum sample pressure. In the case of the PP-DAC, the gasket edge is used for pressure measurement, which corresponds to the lowest sample pressure. The pressures are just given as nominal pressures. Note, however, that at the nominal maximum pressures of 46 and 47 GPa, respectively, the total shift of the {002} peak only differs by ∼2%. This most likely suggests a maximum error in pressure at the maximum pressure of a similar percentage. Note that a past study [18] shows that reversibility is maintained to ∼35 GPa, while compression to above ∼45 GPa results in irreversibility. Both the pan-DAC and the PP-DAC experiment yielded compression well into the irreversibility field.

Both sets of *in situ* XRD measurements were carried out at 30 keV on beamline 16-ID-B at the High Pressure Collaborative Access Team (HPCAT) at the Advanced Photon Source, Argonne National Laboratory. This facility provides a collimated monochromatic x-ray beam with a full width at half maximum (FWHM) of ∼4×6 μm. A 1M Pilatus detector was used in both experiments. The background signal was subtracted from the raw spectra using DIOPTAS 2.3 [21] and peak fitting was performed using the ORIGINPRO 9.1 software package.

III. SIMULATION METHODOLOGY

Molecular dynamics simulations of uniaxial compression were performed to mimic the nonhydrostatic compression in a DAC. An excess uniaxial component is the critical factor to induce the preferred orientation of graphitic layers. While there is also a radial shear component in DAC experiments without a pressure medium, the uniaxial component is, however, key here. Thus, uniaxial compression of a glassy carbon structure in simulation is the closest approach to the experimental compression. First, a realistic GC structure of density 1.5 g/cm^3 and 32 727 atoms was generated via our molecular dynamics methodology [22] using periodic boundary conditions and a cubic simulation box with a side length of 7.58 nm. The structure generated is highly sp^2 bonded, contains entangled graphene layers, and was fully relaxed to ambient. The size of the simulation box is large enough to allow orientation of the

layers in all directions and the Poisson ratio is 0.21; therefore the structure is highly isotropic. In recent work we presented a sensitivity study to evaluate the box size effects on the generated structures, spanning different densities and box sizes, with each series of structures consisting of six repetitions (see Supplemental Material in Ref. [23]). Our methodology yielded highly isotropic structures, with elastic constants, ring statistics, coordination fractions, and mechanical properties of the small structures in good agreement with the larger structures. Subsequently, the structure was uniaxially compressed up to a maximum pressure of 56 GPa using a constant strain rate of $0.0017\,\mathrm{ps}^{-1}$ and allowing 0.1 ps to relax between strains. All simulations were performed using the LAMMPS molecular dynamics package [24] with atomic interactions described by the environment-dependent interaction potential (EDIP) for carbon [25]. Coordination numbers are calculated by counting neighbors within a cutoff distance of 1.85 Å. The diffraction intensity, $I(s)$, in the polycrystalline approximation was computed by the Debye scattering equation [26],

$$I(s) = \sum_{i=1}^{N}\sum_{j=1}^{N} f_i(s) f_j(s) \frac{\sin(2\pi s r_{ij})}{2\pi s r_{ij}},$$

where s is the modulus of the scattering vector, r_{ij} is the distance between two atoms labeled i and j, N is the total number of atoms, and $f(s)$ is the scattering factor for a single carbon atom. To apply this equation and avoid problems caused by the minimum image convention, it is necessary to map the atoms into the primitive cell and treat the structure as an isolated cluster. Localized regions found to adopt the diamond structure are determined using the diamond structure identification tool [27] in the OVITO visualization software [28].

IV. RESULTS AND DISCUSSION

Experimental XRD spectra of GC compressed up to 47 GPa and then recovered back to ambient in the PP-DAC are shown in Fig. 2(a) as a function of Q (where $Q = 2\pi/d$ and d is the d spacing). The uncompressed GC has three major peaks at 1.8, 3.0, and 5.1 Å^{-1} which correspond to the graphitic {002}, {100}, and {110} reflections. Also observed is a minor peak corresponding to the graphitic {004} reflection at 3.6 Å^{-1} and a weak shoulder at 3.1 Å^{-1} corresponding to the {101} reflection. The turbostratic nature of graphitic layer stacking in GC increases the average distance between layers, leading to a lower Q for the center of the {002} peak (at $\sim$1.8 Å^{-1} compared to 1.9 Å^{-1} in graphite), and to a significant reduction in the intensity of the {101} reflection relative to graphite [13].

As the pressure in the PP-DAC increases, the {002} peak shifts significantly upwards in Q, while the {100} peak shifts up only slightly. This result indicates that the average graphitic interlayer spacing (determined by the position of the {002} peak) is more easily deformed than the in-plane spacings (determined by the position of the {100} peak). This is consistent with the XRD results of Lin *et al.* [16] and can be readily explained by the highly anisotropic nature of the Young's modulus in graphite [29]. There is also a noticeable

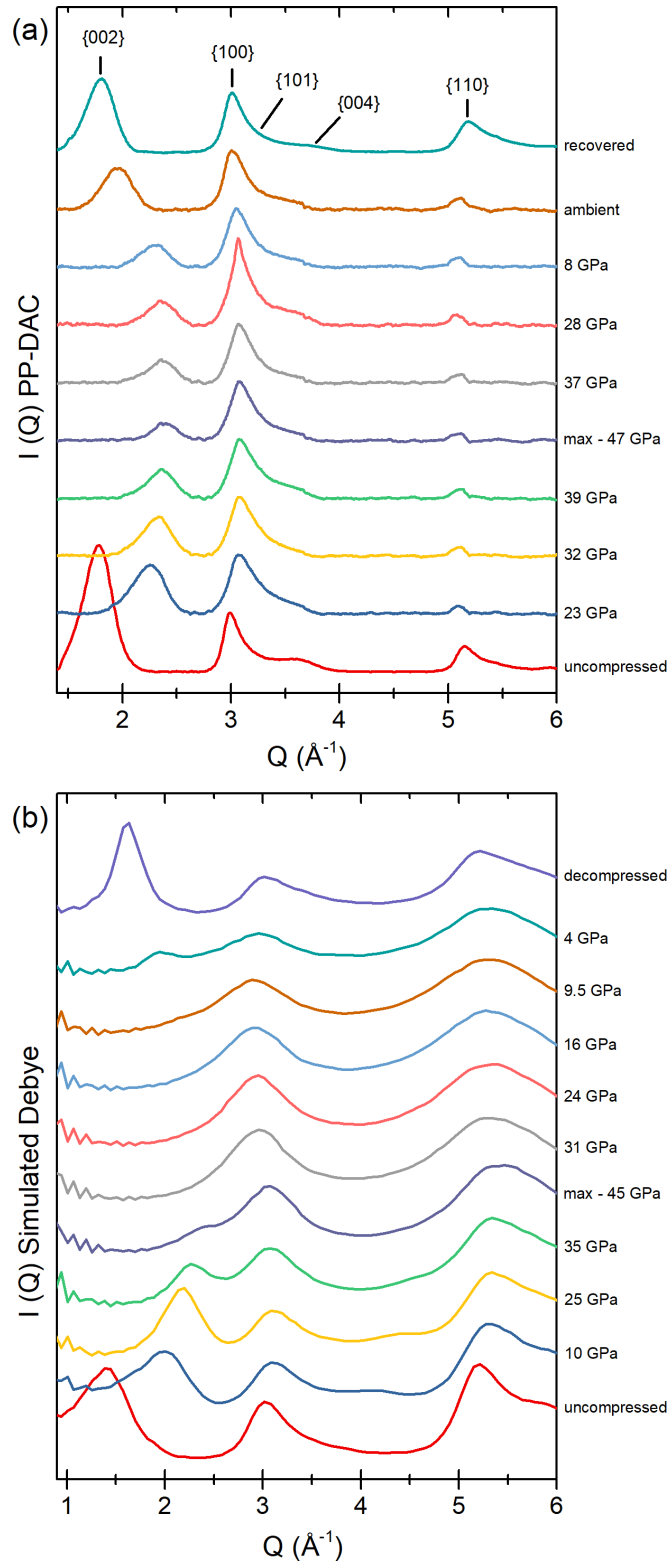

FIG. 2. (a) XRD scans of GC recorded *in situ* in the PP-DAC up to a maximum pressure of 47 GPa. All spectra have been normalized to the intensity of the {100} peak. Note the peak at $\sim$3 Å^{-1} is sharpened in the 28 GPa scan due to the beam clipping the gasket material. For the recovered and uncompressed scans, the samples were removed from the DAC. The major peaks have been indexed to graphite. (b) Diffraction intensity of the simulated GC structure under compression computed using the Debye scattering equation.

decrease in the intensity of the {002} peak relative to the {100} peak. This reduction in the relative intensity can be partially explained by the development of preferred orientation of the graphitic nanostructures under the nonhydrostatic compression (see below). It is also evident that the {002} peak is not shifting at a constant rate with respect to pressure, but at a rate that decreases with pressure, indicating that the material is becoming stiffer. Upon decompression, the {002} peak reverts towards its original position. However, it has a lower intensity due to the development of permanent preferred orientation, as described in our previous work [18].

Raw diffraction patterns of GC at 47 GPa in the PP-DAC and at 46 GPa in the pan-DAC are shown in Figs. 1(b) and 1(d), respectively. At high pressure in the PP-DAC the {002} reflection is circularly symmetric (i.e., there is uniform intensity around the ring). This suggests that when probed with x rays along the compression axis the material is cylindrically isotropic. In contrast, at high pressure in the pan-DAC the {002} reflection exhibits a strongly nonuniform intensity, with high-intensity "arcs" aligned along the compression axis. The development of these arcs demonstrates that the nonhydrostatic compression has resulted in the development of preferred orientation of the graphitic planes in this material. To fully investigate the pressure-driven development of preferred orientation, specific regions of the diffraction patterns [denoted "side area" and "bottom area" as indicated in Figs. 1(b) and 1(d)] were used to generate radially averaged XRD spectra of samples compressed in both DACs.

Figure 3 compares the resulting spectra determined from scattered photons collected on the (a) side and (b) bottom areas of the detector, showing the intensity of the {002} peak as a function of Q recorded under pressure in the PP-DAC. The intensity of the {002} peak is similar in both segments, which indicates a uniformly intense diffraction ring, confirming the random orientation of the nanostructure around the incident beam. The {002} peak position shifts to higher Q with pressure, indicating that the graphitic layers are forced closer together, with the average spacing of ~3.5 Å at ambient being reduced to ~2.7 Å at 47 GPa. Since the graphitic layers contributing to the {002} peak in the PP-DAC are almost parallel to the compression direction, the hydrostatic compression component must be responsible for forcing the layers together.

In contrast, in the pan-DAC there is a clear difference in the intensities of the {002} diffraction ring that falls on the bottom and side areas on the detector as shown in Figs. 3(c) and 3(d). These results show that the intensity of the {002} diffraction ring is not symmetric at high pressure, indicating that the structure is no longer isotropic as there is some level of preferred orientation of graphitic layers, while at low pressure (1 GPa), there is little evidence for preferred orientation in the sample. However, as pressure is increased strong preferred orientation is observed. The intensity of the {002} peak becomes concentrated into two arcs that are symmetrically located along the compression direction [Fig. 1(b)], one of which falls within the bottom area on the detector. These arcs can be explained by the presence of strong alignment of graphitic sheets perpendicular to the compression direction in response to a strong uniaxial component typically present under nonhydrostatic compression in a DAC without a pressure medium. The development of preferred orientation in graphitic materials is frequently observed arising from the minimization of the elastic strain energy [30]. For example, preferred orientation occurs in carbon films

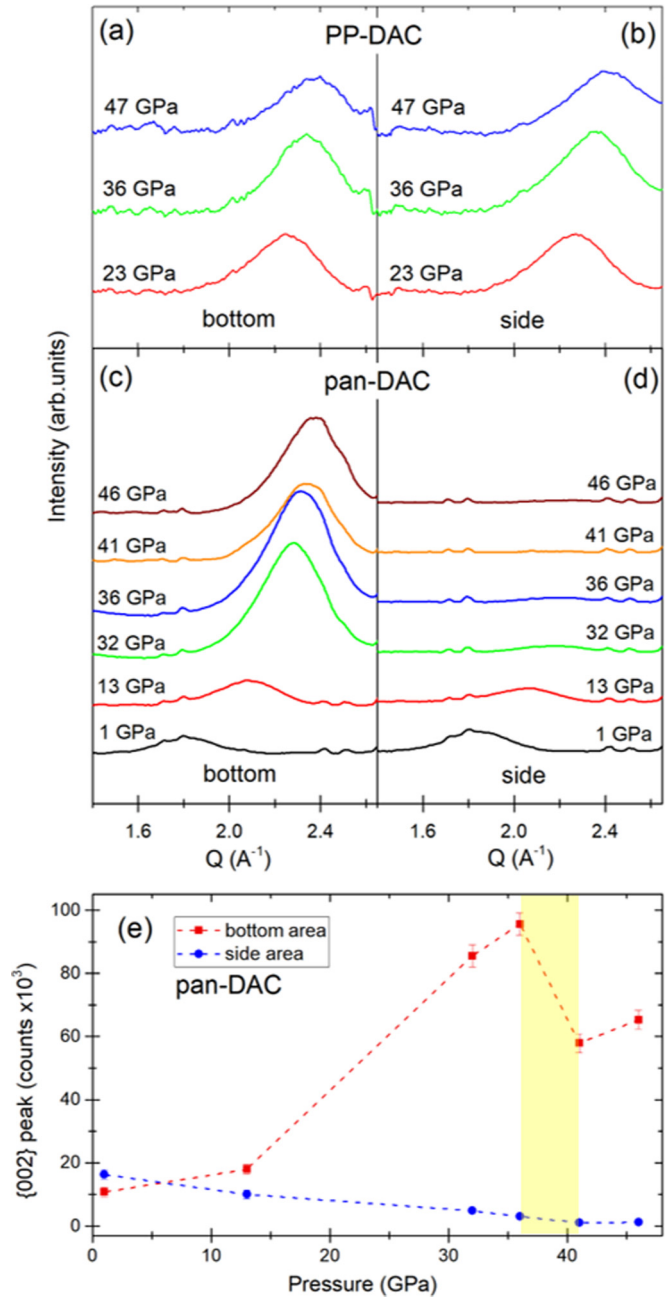

FIG. 3. Selected regions of Q space indexed to the {002} peak of graphite from *in situ* XRD spectra measured in the PP-DAC (a), (b) and the pan-DAC (c), (d) up to a maximum pressure of 47 and 46 GPa, respectively. (e) The intensity of the {002} peak obtained by fitting a Gaussian to the side and bottom spectra shown in (c), (d). This figure shows the gradual onset of preferred orientation of graphitic layers up to 36 GPa, beyond which the {002} peak intensity drops sharply in the bottom direction and is no longer observable in the side direction. The yellow shaded region highlights the pressure range where the sharp change is observed. Error bars fitted in the y-axis direction are calculated from the Gaussian fits.

grown from energetic beams which develop biaxial stress fields [31].

To quantify the degree of preferred orientation, the intensity of the {002} peak was obtained by fitting a Gaussian to the pan-DAC intensity data and the result is shown in Fig. 3(e). Clearly, the intensity of the {002} measured on the side area of the detector [Fig. 3(d)] drops smoothly with increasing pressure. In contrast, the intensity of the {002} on the bottom area of the detector [Fig. 3(c)] increases rapidly as the material is compressed to 36 GPa, then shows a discontinuous fall in intensity at 41 GPa before increasing again. This discontinuity suggests that a structural change has occurred, by analogy with the fall in intensity of the $1s$-π^* peak observed by Mao *et al.* in their inelastic x-ray scattering spectra which they attributed to the sudden buckling of graphitic layers [32] in compressed graphite at ∼16 GPa at room temperature. The higher pressure in GC compared to graphite is required to first orient the graphitic layers before they can be compressed together and buckled.

In order to provide a visual explanation of the transformation of GC under pressure, we have modeled the compression of a GC structure using molecular dynamics. In Fig. 4 we present a series of snapshots showing a 2-nm-thick cross-sectional slab of the simulated structure. This series illustrates the atomic rearrangement that occurs as the GC structure is compressed uniaxially. Figure 4(a) shows the starting structure at ambient where the characteristic features of GC are observed, including a high sp^2 bonding fraction of 95.6% represented by the green atoms and tangled graphitic layers with no preferred orientation. Figures 4(b)–4(f) show the structural development at key stages during compression along the direction indicated by the black arrows. The corresponding pressures and densities are represented alongside each panel. Upon compression, the graphitic layers gradually align perpendicular to the compression axis. This can be seen clearly in Figs. 4(b) and 4(c), and is consistent with the *in situ* XRD data presented in Fig. 3, and in our previous publication [18]. As pressure increases the aligning layers are forced closer together, eventually allowing the formation of cross-links between layers. This phenomenon results in a substantial increase in the sp^3 bonding fraction, as highlighted by the blue atoms in Figs. 4(d)–4(f). At high pressures, over ∼30 GPa, considerable densification of the structure has occurred, reaching 3.24 g/cm^3 at 45 GPa. Note that the densification and formation of a predominantly sp^3 bonded phase occurs while layers are still visible within the structure [Figs. 4(d)–4(f)].

In Fig. 2(b) we compute the diffraction intensity of the simulated structure using the Debye scattering equation at different stages of compression up to 45 GPa and then back to ambient. During compression the {002} peak shifts towards the right and decreases in intensity, similar to the observed progression in the experimental diffraction data shown in Fig. 2(a). The shift of the {002} peak is a result of the layers being forced closer together, which continues up to 45 GPa, beyond which it disappears. On decompression the {002} peak reappears only at low pressure (∼4 GPa), and is almost fully recovered at ambient. It should also be noted that there is significant hysteresis observed in this reversible

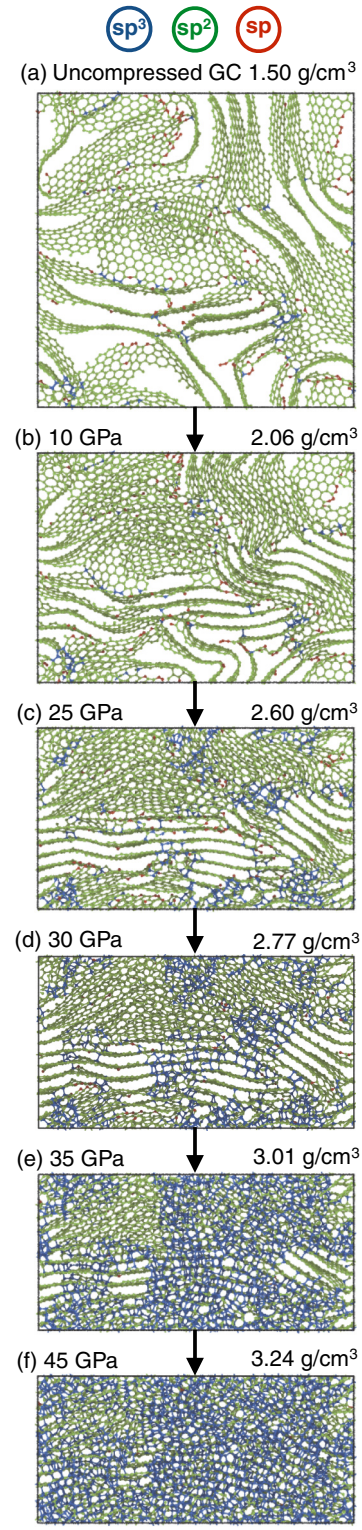

FIG. 4. A sequence of snapshots showing the key stages of the uniaxial compression of GC. The compression axis is parallel to the black arrows. Each snapshot shows a slab of 2 nm depth, where red, green, and blue coloring denote sp, sp^2, and sp^3 bonding, respectively. The pressure at which the structure is compressed, and its corresponding density are indicated on the top of each snapshot. (a) Uncompressed GC structure. The GC structure compressed to (b) 10 GPa, (c) 25 GPa, (d) 30 (e) 35 GPa, and (f) 45 GPa.

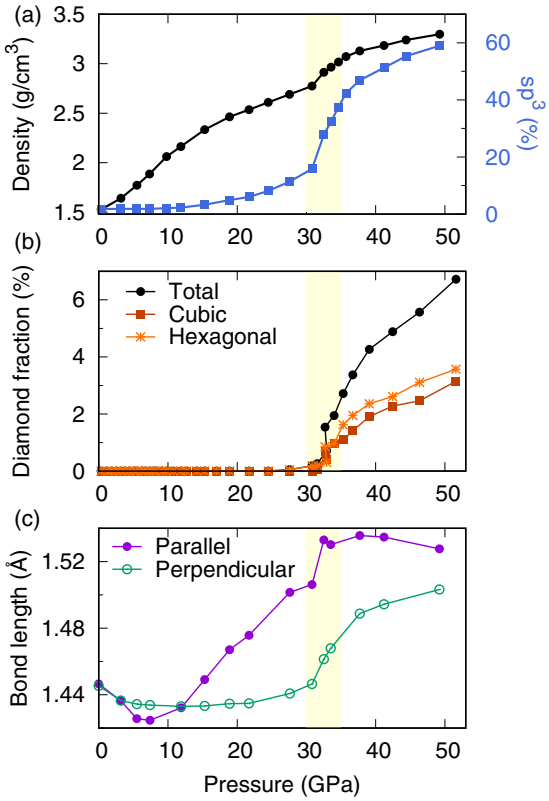

FIG. 5. (a) sp^3 fraction (blue squares, right vertical axis) and the density (black circles, left vertical axis) of the simulated structure as a function of pressure during compression. The yellow shaded region highlights the 30–35 GPa pressure range where the sharp change is observed. (b) Nucleation of diamond crystallites during compression of the simulated structure as a function of pressure. The black circles represent the computed total fraction of atoms in a diamond structure as a function of pressure. The total fraction of diamond is the combination of the fractions of atoms arranged in cubic (brown squares) and hexagonal diamond (orange crosses) structures. (c) Data from the modeling showing the sp^3 bond lengths parallel (purple circles) and perpendicular (blue open circles) to the compression axis.

transformation in both the experimental and simulation data. These simulated diffraction spectra show that the material does recover its graphitic characteristics when returned to ambient. This agrees with the experimental data shown in Fig. 2(a) and the results of our previous publication [18].

In Fig. 5(a) we show the calculated fraction of sp^3 bonding within the simulated structure as a function of pressure. The sp^3 fraction increases gradually during the first stages of compression up to ∼30 GPa, where the compressed structure has a density of ∼2.8 g/cm^3. The sp^3 bonding fraction further increases up to ∼60% at 60 GPa where the density is ∼3.4 g/cm^3. In light of the experimental and simulated results presented here, previous studies on GC under high pressure can now be elucidated further. Lin *et al.* probed a GC sample without a pressure medium using *in situ* XRD from only the standard orientation, i.e., along the compression axis of a DAC (similar to our PP-DAC experiments shown in Fig. 5) [16]. This allowed the observation of peak shifts and the relative peak intensities, but does not give clear evidence of full transition to an sp^3 bonded structure. Additionally, their x-ray Raman spectroscopy results show a decrease in the sp^2 bonding fraction, which they suggest indicates a complete transformation to a fully sp^3 bonded material above ∼40 GPa. Our simulation results support a conversion from sp^2 to sp^3 bonding, but not 100%. In contrast, Solopova *et al.* measured GC using Raman spectroscopy, where the Raman *G* peak (which signifies sp^2 bonded graphitic material) remained up to 60 GPa [17]. Our results support this observation, as a large fraction of sp^2 bonds remain in our simulated structure at 56 GPa. Furthermore, it should be noted that the percentage of sp^3 bonding could still increase gradually with pressure, as sp^3 bonds (in either amorphous or in nanocrystalline form) offer a very weak Raman signal relative to sp^2 [33]. It is also probable that their use of a hydrostatic pressure medium (Ne) suppresses the alignment of graphitic layers, so that they remain in a tangled three-dimensional (3D) matrix and cannot readily form fully sp^3 bonded nanocrystals. Yao *et al.* compressed GC samples in KBr and N_2 pressure media and report that the samples become transparent at ∼30 GPa but only when under an additional excess uniaxial component, i.e., when the sphere bridges the anvils [10]. This result could represent a direct optical observation of the formation of an sp^3 bonded nanocrystalline phase. In fact, the excess uniaxial stress component generated as the sample bridges between the anvils forces the preferred orientation of layers, allowing sp^3 bond formation and nanocrystal nucleation which results in their sample turning transparent. It is also important to consider that the GC precursors used in the experiments of Lin *et al.*, Solopova *et al.*, and Yao *et al.* were purchased from Alfa Aesar, and the GC precursor used in this study was purchased from Hochtemperatur Werkstoffe. This means that there could be some difference in their initial structures at ambient which could influence their behavior at high pressure. Detailed characterization of both varieties of GC is being undertaken but is outside the scope of this manuscript.

Figure 5(a) shows a sudden increase in density and in the fraction of sp^3 bonded atoms in the compressed structure occurring at 30–35 GPa, as indicated by the yellow shaded region. This pressure threshold represents the onset of formation of an sp^3 bonded phase coexisting with the stacked and oriented layers, and is initiated by cross-linking between layers. We observe that above this pressure threshold in some small localized regions the sp^3 bonded atoms are able to arrange themselves into a diamond structure. To quantify the nucleation of diamond crystallites within the compressed GC structure, we show in Fig. 5(b) the fraction of sp^3 bonded atoms that have adopted a diamond structure, including both cubic and hexagonal lattice types. The nucleation of the small diamond crystallites begins at ∼30 GPa, precisely where the sharp increases in sp^3 bonding and density are observed [Fig. 5(a)]. As the pressure increases beyond 30 GPa the diamond crystallite fraction quickly increases and reaches ∼7% at a pressure of ∼50 GPa, with approximately equal contributions from cubic and hexagonal diamond phases. Note that at ∼50 GPa nearly 60% of atoms are sp^3 bonded, but the fraction of atoms which have adopted a diamond crystallite structure is only a small percentage, roughly 7%. To determine the structural configuration of the majority of the sp^3 bonds that are not present in crystallites, we calculated

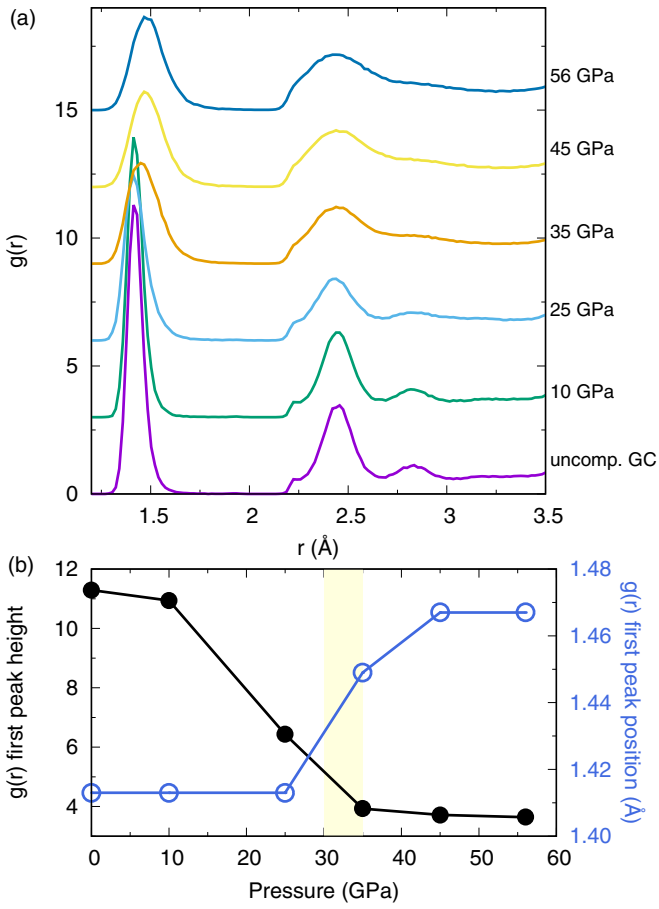

FIG. 6. (a) Radial distribution functions of the uncompressed simulated GC structure, and of the compressed structure at 10, 25, 35, 45, and 56 GPa. (b) Left axis: First neighbor peak intensity from the $g(r)$ curves in (a) as a function of density during compression. Data are represented in black circles. Right axis: First neighbor peak position from the $g(r)$ curves in (a) as a function of density during compression. Data are represented in blue open circles. The yellow shaded region highlights the 30–35 GPa pressure range where the sharp change is observed in Fig. 5.

the average sp^3 bond length for bonds within 20° of the compression axis and the same average for bonds within 20° of the direction perpendicular to the compression axis. The bond length averages and their difference are shown in Fig. 5(c) as a function of pressure. The results show a clear difference in the bond lengths occurs at higher pressures, with the bonds aligned parallel to the compression axis being longer. In the vicinity of 35 GPa, the bond length difference reaches a maximum. This result is characteristic of many structures that are proposed to form from graphitic precursors under high pressure at room temperature [1], such as *M*-carbon [4], *W*-carbon [5], and bct-4-carbon [6] which all exhibit two distinct sp^3 bond lengths. The higher threshold pressure observed for GC arises due to the need to first orientate the graphitic layers prior to any transformation to an sp^3 bonded structure.

In Fig. 6(a) we present the radial distribution functions, $g(r)$, of the uncompressed simulated GC structure and at key steps during compression. From the $g(r)$ curves, information from the first neighbor peak is extracted and plotted as a function of pressure and density during compression [Fig. 6(b)]. As observed in Fig. 6(a), the uncompressed structure shows a narrow and sharp first neighbor peak very close to the graphite distance, indicating a large sp^2 bonding fraction. Upon compression, a sudden shift in the position of the first peak occurs and the intensity drops between 25 and 35 GPa. This behavior corresponds to a change in the materials nanostructure. Broader peaks indicate a higher degree of disorder, while the upshift in peak position is due to the increase in the fraction of sp^3 bonded atoms.

Finally, it is interesting to discuss the implications and uses of forming a high-pressure sp^3 bonded crystalline phase from GC. It appears that the sp^3 bonded phase and nanocrystalline diamonds formed at high pressure are not recoverable at ambient where graphite is the thermodynamically stable phase [18]. However, we have shown in a recent publication that annealing this phase at 400 °C adds enough energy for the diamond nanocrystals to properly form, where they are recoverable at ambient [34,35]. Other recent work has shown that at lower pressure but with somewhat elevated temperature (400 °C–1000 °C) small percentages of sp^3 bonds can be retained to ambient [36]. Additionally, compression to 50 GPa and exposures to more extreme temperatures (1800 K) via laser heating results in a recoverable amorphous diamondlike material that is ∼100% sp^3 bonded being recovered [37]. Furthermore, studying subtle structural details of this nanocrystalline phase at high pressure is difficult due to the low x-ray scattering cross section of carbon. To provide structural details of this phase it may be necessary to further study this phase transformation with different *in situ* measurement techniques such as high-pressure neutron diffraction [38].

V. CONCLUSION

The experimental and simulation data presented here reveal insights into the phase behavior of GC under compression at room temperature. The compression of GC under nonhydrostatic compression using *in situ* XRD with two orthogonal beam orientations was investigated. The results show the gradual development of strong preferred orientation of graphitic nanostructures up to ∼35 GPa and evidence for a major structural change at this pressure. The experimental results were supported with molecular dynamics simulations which revealed how the atomic level nanostructure evolved with pressure. This includes a gradual increase in the sp^3 bonding fraction up to ∼30–35 GPa, before a sharp increase in the number of sp^3 bonds is observed concurrently with the onset of sp^3 bonded nanocrystalline diamonds. The nanostructure above this threshold also contains a high proportion of atoms bonded in configurations which have two distinct sp^3 bond lengths, consistent with many proposed high-pressure carbon structures.

The Department of Energy will provide public access to these results of federally sponsored research in accordance with the DOE Public Access Plan [39].

ACKNOWLEDGMENTS

J.E.B. would like to acknowledge the Australian Research Council (ARC) for financial support through a Future

Fellowship (Grant No. FT130101355). J.E.B. and D.G.M. acknowledge funding under the ARC Discovery Project scheme (Grant No. DP140102331). B.H. acknowledges funding through the ORNL Neutron Scattering Facilities, DOE Office of Science User Facilities operated by the Oak Ridge National Laboratory. N.A.M. acknowledges financial support through a fellowship, Grant No. FT120100924. I.S.-M. acknowledges financial support through a fellowship, Grant No. FT140100191. Work by R.B. was supported by the Energy Frontier Research in Extreme Environments (EFree) Center, an Energy Frontier Research Center funded by the U.S. Department of Energy (DOE), Office of Science, Basic Energy Sciences (BES) under Award No. DE-SC0001057. Computational resources are provided by the Pawsey Supercomputing Centre with funding from the Australian Government and the Government of Western Australia. The XRD measurements presented here were performed at HPCAT (Sector 16), Advanced Photon Source (APS), Argonne National Laboratory. HPCAT operations are supported by DOE-NNSA under Award No. DE-NA0001974, with partial instrumentation funding by NSF. The Advanced Photon Source is a U.S. Department of Energy (DOE) Office of Science User Facility operated for the DOE Office of Science by Argonne National Laboratory under Contract No. DE-AC02-06CH11357.

This work has been partially supported by the U.S. Department of Energy. ORNL is managed by UT-Battelle, LLC, under Contract No. DE-AC05-00OR22725 for the U.S. Department of Energy. The United States Government retains and the publisher, by accepting the article for publication, acknowledges that the United States Government retains a nonexclusive, paid-up, irrevocable, worldwide license to publish or reproduce the published form of this manuscript, or allow others to do so, for U.S. Government purposes.

[1] Y. Wang and K. K. M. Lee, From soft to superhard: Fifty years of experiments on cold-compressed graphite, J. Superhard Mater. **34**, 360 (2012).

[2] A. R. Oganov, R. J. Hemley, R. M. Hazen, and A. P. Jones, Structure, bonding, and mineralogy of carbon at extreme conditions, Rev. Mineral. Geochem. **75**, 47 (2013).

[3] W. Utsumi and T. Yagi, Light-transparent phase formed by room-temperature compression of graphite, Science **252**, 1542 (1991).

[4] Q. Li, Y. Ma, A. R. Oganov, H. Wang, H. Wang, Y. Xu, T. Cui, H. K. Mao, and G. Zou, Superhard Monoclinic Polymorph of Carbon, Phys. Rev. Lett. **102**, 175506 (2009).

[5] J. T. Wang, C. Chen, and Y. Kawazoe, Low-Temperature Phase Transformation from Graphite to sp^3 Orthorhombic Carbon, Phys. Rev. Lett. **106**, 075501 (2011).

[6] K. Umemoto, R. M. Wentzcovitch, S. Saito, and T. Miyake, Body-Centered Tetragonal C_4: A Viable sp^3 Carbon Allotrope, Phys. Rev. Lett. **104**, 125504 (2010).

[7] Q. Zhu, Q. Zeng, and A. R. Oganov, Systematic search for low-enthalpy sp^3 carbon allotropes using evolutionary metadynamics, Phys. Rev. B **85**, 201407 (2012).

[8] Z. Zhao, B. Xu, X. F. Zhou, L. M. Wang, B. Wen, J. He, Z. Liu, H. T. Wang, and Y. Tian, Novel Superhard Carbon: C-Centered Orthorhombic C_8, Phys. Rev. Lett. **107**, 215502 (2011).

[9] M. Amsler, J. A. Flores-Livas, L. Lehtovaara, F. Balima, S. A. Ghasemi, D. MacHon, S. Pailhes, A. Willand, D. Caliste, S. Botti, A. San Miguel, S. Goedecker, and M. A. L. Marques, Crystal Structure of Cold Compressed Graphite, Phys. Rev. Lett. **108**, 065501 (2012).

[10] M. Yao, X. Fan, W. Zhang, Y. Bao, R. Liu, B. Sundqvist, and B. Liu, Uniaxial-stress-driven transformation in cold compressed glassy carbon, Appl. Phys. Lett. **111**, 101901 (2017).

[11] Y. Wang, J. E. Panzik, B. Kiefer, and K. K. M. Lee, Crystal structure of graphite under room-temperature compression and decompression, Sci. Rep. **2**, 520 (2012).

[12] S. E. Boulfelfel, A. R. Oganov, and S. Leoni, Understanding the nature of "superhard graphite", Sci. Rep. **2**, 471 (2012).

[13] G. M. Jenkins and K. Kawamura, Structure of glassy carbon, Nature **231**, 175 (1971).

[14] P. J. F. Harris, Fullerene-related structure of commercial glassy carbons, Philos. Mag. **84**, 3159 (2004).

[15] Z. Zhao, E. F. Wang, H. Yan, Y. Kono, B. Wen, L. Bai, F. Shi, J. Zhang, C. Kenney-Benson, C. Park, Y. Wang, and G. Shen, Nanoarchitectured materials composed of fullerene-like spheroids and disordered graphene layers with tunable mechanical properties, Nat. Commun. **6**, 6212 (2015).

[16] Y. Lin, L. Zhang, H. K. Mao, P. Chow, Y. Xiao, M. Baldini, J. Shu, and W. L. Mao, Amorphous Diamond: A High-Pressure Superhard Carbon Allotrope, Phys. Rev. Lett. **107**, 175504 (2011).

[17] N. A. Solopova, N. Dubrovinskaia, and L. Dubrovinsky, Raman spectroscopy of glassy carbon up to 60 GPa, Appl. Phys. Lett. **102**, 121909 (2013).

[18] T. B. Shiell, D. G. McCulloch, D. R. McKenzie, M. R. Field, B. Haberl, R. Boehler, B. A. Cook, C. de Tomas, I. Suarez-Martinez, N. A. Marks, and J. E. Bradby, Graphitization of Glassy Carbon after Compression at Room Temperature, Phys. Rev. Lett. **120**, 215701 (2018).

[19] R. Boehler, New diamond cell for single-crystal x-ray diffraction, Rev. Sci. Instrum. **77**, 115103 (2006).

[20] H. K. Mao, J. Xu, and P. M. Bell, Calibration of the ruby pressure gauge to 800 kbar under quasi-hydrostatic conditions, J. Geophys. Res. **91**, 4673 (1986).

[21] C. Prescher and V. B. Prakapenka, DIOPTAS: a program for reduction of two-dimensional x-ray diffraction data and data exploration, High Press. Res. **35**, 223 (2015).

[22] C. de Tomas, I. Suarez-Martinez, and N. A. Marks, Graphitization of amorphous carbons: A comparative study of interatomic potentials, Carbon **109**, 681 (2016).

[23] C. de Tomas, I. Suarez-Martinez, and N. A. Marks, Carbide-derived carbons for dense and tunable 3D graphene networks, Appl. Phys. Lett. **112**, 251907 (2018).

[24] S. Plimpton, Fast parallel algorithms for short-range molecular dynamics, J. Comput. Phys. **117**, 1 (1995).

[25] N. A. Marks, Generalizing the environment-dependent interaction potential for carbon, Phys. Rev. B **63**, 035401 (2000).

[26] B. E. Warren, *X-Ray Diffraction* (Addison-Wesley Publishing Co., Reading, MA, 1969).

[27] E. Maras, O. Trushin, A. Stukowski, T. Ala-Nissila, and H. Jónsson, Global transition path search for dislocation formation in Ge on Si(001), Comput. Phys. Commun. **205**, 13 (2016).

[28] A. Stukowski, Visualization and analysis of atomistic simulation data with OVITO-the Open Visualization Tool, Modell. Simul. Mater. Sci. Eng. **18**, 015012 (2010).

[29] B. T. Kelly, *Physics of Graphite* (Applied Science, London, 1981).

[30] L. C. F. Blackman and A. R. Ubbelohde, Stress recrystallization of graphite, Proc. R. Soc. London, Ser. A **266**, 20 (1962).

[31] D. W. M. Lau, J. G. Partridge, M. B. Taylor, D. G. McCulloch, J. Wasyluk, T. S. Perova, and D. R. McKenzie, Microstructural investigation supporting an abrupt stress induced transformation in amorphous carbon films, J. Appl. Phys. **105**, 084302 (2009).

[32] W. L. Mao, H. Mao, P. J. Eng, T. P. Trainor, M. Newville, C. Kao, D. L. Heinz, J. Shu, Y. Meng, and R. J. Hemley, Bonding changes in compressed superhard graphite, Science **302**, 425 (2003).

[33] A. C. Ferrari, Determination of bonding in diamond-like carbon by Raman spectroscopy, Diam. Relat. Mater. **11**, 1053 (2002).

[34] T. B. Shiell, D. G. McCulloch, J. E. Bradby, B. Haberl, R. Boehler, and D. R. McKenzie, Nanocrystalline hexagonal diamond formed from glassy carbon, Sci. Rep. **6**, 37232 (2016).

[35] S. Wong, T. B. Shiell, B. A. Cook, J. E. Bradby, D. R. McKenzie, and D. G. McCulloch, The transformation pathway from glassy carbon to hexagonal diamond, Carbon **142**, 475 (2018).

[36] M. Hu, J. He, Z. Zhao, T. A. Strobel, W. Hu, D. Yu, H. Sun, L. Liu, Z. Li, M. Ma, Y. Kono, J. Shu, H.-K. Mao, Y. Fei, G. Shen, Y. Wang, S. J. Juhl, J. Y. Huang, Z. Liu, B. Xu, and Y. Tian, Compressed glassy carbon: An ultrastrong and elastic interpenetrating graphene network, Sci. Adv. **3**, e1603213 (2017).

[37] Z. Zeng, L. Yang, Q. Zeng, H. Lou, H. Sheng, J. Wen, D. J. Miller, Y. Meng, W. Yang, W. L. Mao, and H. K. Mao, Synthesis of quenchable amorphous diamond, Nat. Commun. **8**, 322 (2017).

[38] R. Boehler, J. J. Molaison, and B. Haberl, Novel diamond cells for neutron diffraction using multi-carat CVD anvils, Rev. Sci. Instrum. **88**, 083905 (2017).

[39] http://energy.gov/downloads/doe-public-access-plan.